Homography VAE: Automatic Bird's Eye View Image Reconstruction from Multi-Perspective Views

Keisuke Toida[1][a], Naoki Kato[2][b], Osamu Segawa[2][c], Takeshi Nakamura[2][d] and Kazuhiro Hotta[1][e]

[1]*Meijo University, 1-501 Shiogamaguchi, Tempaku-ku, Nagoya 468-8502, Japan*

[2]*Chubu Electric Power Co., Inc., 1-1 Higashishin-cho, Higashi-ku, Nagoya 461-8680, Japan*

Keywords: Variational Autoencoder, Homography Transformation, Unsupervised Learning.

Abstract: We propose Homography VAE, a novel architecture that combines Variational AutoEncoders with Homography transformation for unsupervised standardized view image reconstruction. By incorporating coordinate transformation into the VAE framework, our model decomposes the latent space into feature and transformation components, enabling the generation of consistent standardized view from multi-viewpoint images without explicit supervision. Effectiveness of our approach is demonstrated through experiments on MNIST and GRID datasets, where standardized reconstructions show significantly improved consistency across all evaluation metrics. For the MNIST dataset, the cosine similarity among standardized view achieved 0.66, while original and transformed views show 0.29 and 0.37, respectively. The number of PCA components required to explain 95% of the variance decreases from 193.5 to 33.2, indicating more consistent representations. Even more pronounced improvements are observed on GRID dataset, in which standardized view achieved a cosine similarity of 0.92 and required only 7 PCA components compared to 167 for original images. Furthermore, the first principal component of standardized view explains 71% of the total variance, suggesting highly consistent geometric patterns. These results validate that Homography VAE successfully learns to generate consistent standardized view representations from various viewpoints without requiring ground truth Homography matrices.

1 INTRODUCTION

In recent years, the importance of techniques for transforming images captured from various viewpoints into a standardized perspective has grown significantly in fields such as autonomous driving and surveillance camera systems. Bird's Eye View (BEV), which provides a top-down perspective of a scene, is particularly important for these applications as it enables better understanding of spatial relationships and object positions. Although Homography transformation has been widely used for such viewpoint transformations, manual estimation of Homography parameters requires significant human effort and expertise, making it impractical for large-scale applications. In the field of deep learning, Variational Autoencoders (VAE) (Kingma and Welling, 2014) have demonstrated excellent performance in image generation and reconstruction. Although VAEs can encode input data into a low-dimensional latent space and reconstruct the original data from it, conventional VAEs struggle to directly reconstruct standardized view images from perspective-transformed images.

To address this limitation and enable unsupervised learning of viewpoint transformations, we propose Homography VAE, a novel architecture that incorporates Homography transformation into the VAE framework through coordinate transformation. Our model learns to decompose the latent space into feature and transformation components, enabling the reconstruction of both input and standardized view using a single framework.

We demonstrated the effectiveness of our proposed method through experiments on the MNIST and synthetic GRID datasets. Our results show that the proposed method successfully generates consistent standardized view reconstructions, achieving

[a] https://orcid.org/0009-0006-4873-3651
[b] https://orcid.org/0009-0004-3815-0829
[c] https://orcid.org/0009-0000-2469-6098
[d] https://orcid.org/0009-0001-4991-3383
[e] https://orcid.org/0000-0002-5675-8713

Toida, K., Kato, N., Segawa, O., Nakamura, T. and Hotta, K.
Homography VAE: Automatic Bird's Eye View Image Reconstruction from Multi-Perspective Views.
DOI: 10.5220/0013244800003912

In *Proceedings of the 20th International Joint Conference on Computer Vision, Imaging and Computer Graphics Theory and Applications (VISIGRAPP 2025) - Volume 3: VISAPP*, pages 626-632
ISBN: 978-989-758-728-3; ISSN: 2184-4321

higher pairwise cosine similarity and lower L2 distance compared to input and transformed views. Furthermore, the significant reduction in PCA components indicates the model's ability to learn compact and consistent representations.

This paper is organized as follows. Section 2 reviews related works in variational autoencoders and Homography estimation. Section 3 describes the details of our proposed method. Section 4 presents experimental results and analysis. Finally, Section 5 concludes our paper.

2 RELATED WORKS

The research related to our work involves variational autoencoders, transformation-aware autoencoders, and deep learning-based Homography estimation. VAE(Kingma and Welling, 2014) combines variational inference with deep neural networks to learn latent representations of data. This framework has been widely adopted for various image generation and reconstruction tasks. β-VAE(Higgins et al., 2017) extends this framework by introducing a hyperparameter to control the capacity of the latent bottleneck. In the context of transformation-aware architectures, Affine VAE(Bidart and Wong, 2019) incorporates affine transformation awareness into the VAE framework, demonstrating improved generalization and robustness to distribution shifts. Similarly, Spatial Transformer Networks(Jaderberg et al., 2015) introduced a differentiable module for spatial transformations within neural networks though not specifically in a VAE context.

In the field of Homography estimation, deep learning approaches have shown promising results. Deep Image Homography Estimation(DeTone et al., 2016) demonstrated the first successful application of deep learning to direct Homography parameter estimation from image pairs. This approach was extended to dynamic scenes(Le et al., 2020), incorporating temporal consistency. Self-supervised approaches(Wang et al., 2019) have further eliminated the need for manual annotations in Homography estimation.

However, these existing approaches have several limitations. Deep learning-based methods typically require ground truth Homography matrices for training, which are often costly to obtain. Furthermore, while various methods have been proposed for Homography estimation or image transformation, none have specifically addressed the challenge of reconstructing standardized view images from multi-viewpoint datasets without explicit supervision. Our proposed Homography VAE addresses these limitations by incorporating Homography transformation into the VAE framework, enabling unsupervised learning of viewpoint transformations.

3 PROPOSED METHOD

We propose Homography VAE, a novel architecture that combines VAE with Homography transformation to enable standardized view image reconstruction from multi-viewpoint images. As shown in Figure 1, our method consists of three main components: an encoder for latent representation, a Homography transformation module, and a decoder for image reconstruction.

3.1 Model Architecture

3.1.1 Image Encoder

Let $x \in \mathbb{R}^{H \times W \times C}$ be an input image captured from an arbitrary viewpoint, where H, W, and C denote the height, width, and number of channels respectively. The encoder $E(\cdot)$ maps x to a latent representation z.

$$z = E(x) \tag{1}$$

The latent space z is designed to contain both image feature information and Homography parameters. Specifically, we partition z into two parts.

$$z = [z_{feat}, z_{homo}] \tag{2}$$

where $z_{feat} \in \mathbb{R}^d$ represents d-dimensional image features and $z_{homo} \in \mathbb{R}^8$ contains the information for computing the Homography transformation matrix $H \in \mathbb{R}^{3\times3}$.

3.1.2 Homography Transformation Module

From z_{homo}, we compute the Homography transformation matrix H that represents the viewpoint transformation from the standard coordinate system to the input image's perspective. A Homography transformation can be represented by a 3×3 matrix.

$$H = \begin{bmatrix} h_{11} & h_{12} & h_{13} \\ h_{21} & h_{22} & h_{23} \\ h_{31} & h_{32} & h_{33} \end{bmatrix} \tag{3}$$

where h_{33} is typically set to 1 as the matrix is defined up to a scale factor. The standard coordinates C_{std} are defined as a regular grid in normalized coordinates.

$$C_{std} := \{x \in \mathbb{R}^{3\times h\times w} | -1 \leq x \leq 1\} \tag{4}$$

For a point in homogeneous coordinates $p = (x,y,1)^\top$, the transformation is computed by Equation 5.

$$p' = Hp = (x', y', w')^\top \tag{5}$$

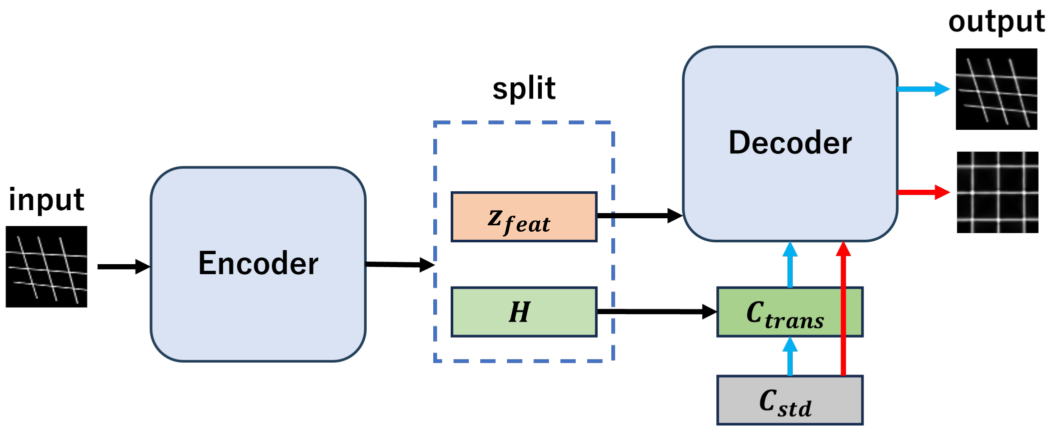

Figure 1: Overview of Homography VAE architecture. The encoder maps input images to a latent representation that is split into feature and transformation components. The decoder employs a dual-branch strategy: the first branch (blue arrow) uses transformed coordinates C_{trans} to reconstruct the input viewpoint, while the second branch (red arrow) uses standard coordinates C_{std} to generate the standardized view. Both branches share the same feature representation z_{feat} but use different coordinate information.

The homogeneous coordinates are converted back to Euclidean coordinates through perspective division in Equation 6.

$$(x'', y'') = (\frac{x'}{w'}, \frac{y'}{w'}) \tag{6}$$

Applying these transformations to all points in C_{std}, we obtain the transformed coordinates C_{trans}.

$$C_{trans} = H \cdot C_{std} \tag{7}$$

3.1.3 Decoder and Image Reconstruction

The decoder $D(\cdot)$ takes both the image features z_{feat} and coordinate information to reconstruct the image. For reconstructing the input viewpoint image, we use

$$x_{rec} = D(z_{feat}, C_{trans}). \tag{8}$$

To reconstruct the standardized view image, we use the standard coordinates C_{std} instead of the transformed coordinates.

$$x_{std} = D(z_{feat}, C_{std}) \tag{9}$$

This key feature allows our model to reconstruct standardized view images without explicit supervision of the transformation parameters. The decoder learns to associate the standard coordinate system with the standardized view perspective through the training process.

3.2 Training Objective

The model is trained using the standard VAE objective function with a reconstruction loss and KL divergence term.

$$\mathcal{L}(\theta, \phi; x, z) = \mathbb{E}_{q_\phi(z|x)}[\log p_\theta(x|z)] - D_{\mathrm{KL}}(q_\phi(z|x)||p(z)) \tag{10}$$

where $q_\phi(z|x)$ and $p_\theta(x|z)$ denote the encoder and decoder distributions respectively, with $p(z) = \mathcal{N}(0,1)$. Here, ϕ and θ are learnable parameters of the neural networks. The encoder $q_\phi(z|x)$ outputs parameters of a Gaussian distribution $\mathcal{N}(\mu_\phi(x), \sigma^2_\phi(x))$, where $\mu_\phi(x)$ and $\sigma^2_\phi(x)$ are learned through the neural network. The KL divergence term D_{KL} measures the difference between the encoder's distribution and the prior distribution $p(z)$.

The key advantage of our proposed method is that it learns to estimate Homography transformations in an unsupervised manner while simultaneously encoding image features in the latent space. By decomposing the latent representation into feature and transformation components, the model can reconstruct images from both the input and standardized view using a single framework. This unified approach enables viewpoint transformation without requiring ground truth Homography matrices during training.

4 EXPERIMENTS

4.1 Datasets

We evaluate our proposed method on two different datasets. The first dataset is MNIST, which consists of handwritten digits with a resolution of 28×28 pixels. The second dataset comprises synthetically generated GRID images with a resolution of 64×64 pixels containing grid patterns. For both datasets, we apply random Homography transformations to the original images during training and testing to simulate multi-viewpoint inputs.

Table 1: Detailed evaluation results for each digit class in MNIST dataset. Mean ± std are shown for cosine similarity and L2 distance.

Class	Original			Transformed			Standardized		
	Cos.Sim.	L2 Dist.	PCA	Cos.Sim.	L2 Dist.	PCA	Cos.Sim.	L2 Dist.	PCA
0	0.31±0.14	13.49±1.75	185	0.38±0.16	11.75±1.94	59	0.69±0.15	8.86±2.20	26
1	0.22±0.20	9.44±1.62	154	0.25±0.22	8.34±1.68	47	0.75±0.13	4.96±1.47	23
2	0.30±0.13	12.58±1.59	207	0.39±0.16	10.25±1.77	65	0.62±0.13	8.68±1.86	39
3	0.29±0.14	12.25±1.57	205	0.38±0.16	9.76±1.68	68	0.62±0.14	8.15±1.74	38
4	0.30±0.13	11.36±1.46	202	0.39±0.16	8.97±1.54	61	0.65±0.13	6.92±1.49	35
5	0.27±0.12	11.91±1.52	203	0.37±0.14	9.38±1.59	65	0.58±0.15	7.79±1.68	35
6	0.32±0.14	12.11±1.60	188	0.41±0.16	10.19±1.78	62	0.65±0.15	8.17±1.91	32
7	0.26±0.15	11.22±1.56	187	0.32±0.17	9.44±1.67	56	0.64±0.16	7.14±1.72	31
8	0.35±0.13	12.21±1.56	210	0.46±0.16	9.58±1.77	69	0.69±0.10	7.33±1.64	40
9	0.31±0.14	11.35±1.45	194	0.39±0.16	9.39±1.52	68	0.66±0.13	7.42±1.56	33

4.2 Implementation Details

The encoder and decoder networks are implemented using convolutional neural networks. We train our model using the Adam optimizer with a learning rate of 0.001. To stabilize the training, we employ cyclic KL annealing (Fu et al., 2019) for mitigating KL collapse and gradient clipping (Pascanu et al., 2013) with a maximum norm of 1.0. During training and testing, we randomly sample Homography transformation parameters within a predetermined range to generate diverse viewpoint variations. Specifically, we perturb the four corner points of the input image with random displacements to create the transformation matrix. The input image is then warped using homography transformation with the obtained transformation matrix.

4.3 Evaluation Metrics

To quantitatively evaluate the effectiveness of our model, we employ four metrics to assess the consistency of the reconstructed images within each class. First, we compute the mean pairwise cosine similarity, measuring the average directional similarity between image pairs. Second, we calculate the mean pairwise L2 distance to quantify pixel-level differences between images. Third, we analyze the number of principal components required to explain 95% of the total variance in the PCA space, where fewer components indicate more compact representations. Finally, we evaluate the first principal component ratio, which quantifies how much of the total variance is captured by the most significant direction of variation. All metrics are computed separately for original, transformed, and standardized images to enable comprehensive comparison.

4.4 Results and Analysis

Our experimental results on MNIST dataset demonstrate that the standardized view reconstructions achieve significantly higher consistency compared to both original and transformed images, as shown in Table 1 and 2. The comparison can be analyzed from three perspectives. First, the cosine similarity metric indicates that standardized view maintain higher directional consistency across samples compared to both original and transformed images. Second, the lower L2 distance in standardized view suggests that our model successfully reduces pixel-wise variations while preserving essential image features. Third, the analysis of PCA components reveals that standardized view can be represented in a significantly lower-dimensional space compared with original and transformed images, indicating that our model successfully learns to generate consistent standardized view reconstructions.

Notably, this improvement in consistency is observed across all digit classes in the MNIST dataset, as detailed in Table 2. The standardized view consistently show better performance in all metrics, with particularly strong results for simpler digits such as "1". Even for more complex digits with higher inherent variability, our model maintains improved consistency while preserving the distinctive features of each class.

Furthermore, we evaluated our model on the synthetic GRID dataset, which contains more structured patterns than MNIST. As shown in Table 3, the results on GRID images demonstrate even more pronounced improvements in the standardized view reconstructions. While the performance on MNIST is relatively lower compared to GRID dataset, this is primarily because the MNIST model needs to handle multiple digit classes simultaneously. This requires the model to learn class-specific features along with viewpoint transformations. In contrast, GRID

Table 2: Comparison of average metrics across different reconstruction types on MNIST dataset.

Metric	Original	Transformed	Standardized
Cosine Similarity ↑	0.29	0.37	0.66
L2 Distance ↓	11.79	9.70	7.54
PCA Components ↓	193.50	62.00	33.20
First Component Ratio ↑	0.11	0.15	0.22

Table 3: Comparison of average metrics across different reconstruction types on GRID dataset.

Metric	Original	Transformed	Standardized
Cosine Similarity ↑	0.15±0.05	0.24±0.06	0.92±0.09
L2 Distance ↓	19.86±1.05	16.53±1.10	5.78±2.99
PCA Components ↓	167	156	7
First Component Ratio ↑	0.03	0.04	0.71

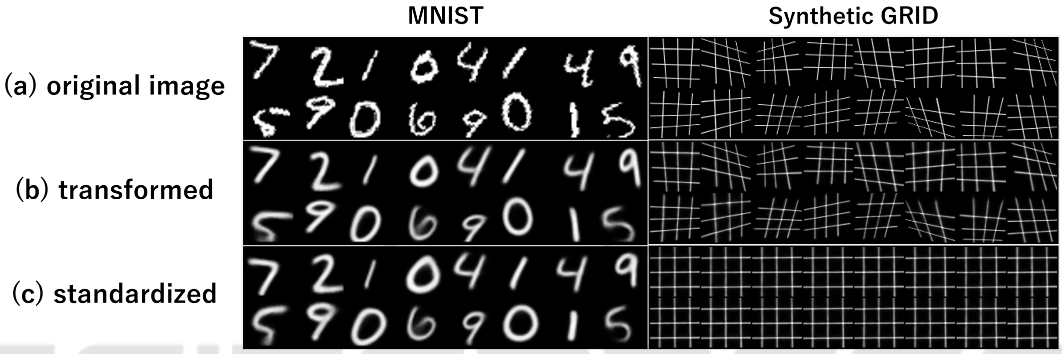

Figure 2: Qualitative results of image reconstruction. For each dataset, we show (a) original input images with various viewpoint transformations, (b) transformed view reconstructions that preserve the input perspective, and (c) standardized view reconstructions that consistently align to a frontal viewpoint regardless of input variations. Left column shows the results on MNIST dataset. Right column shows the results on GRID dataset. Our model successfully generates consistent standardized view while maintaining the structural integrity of the patterns.

dataset contains only single-class patterns, allowing the model to focus solely on learning viewpoint transformations. Particularly notable is the dramatic reduction in required PCA components, indicating that our model achieves remarkably consistent standardized view reconstructions for structured grid patterns. The high cosine similarity and low L2 distance of standardized view further support this finding.

The qualitative results shown in Figure 2 demonstrate our model's ability to generate visually consistent reconstructions. Although the transformed views accurately preserve the perspective of input images, the standardized view exhibit consistent frontal representations regardless of the input viewpoint. Figure 3 shows the reconstruction results specifically for MNIST digit ”4”. Despite its relatively complex structure, our model successfully generates consistent standardized view while preserving the features of this digit class.

The consistency of these reconstructions is quantitatively validated through pairwise cosine similarity analysis. Figure 4 visualizes the similarity matrices computed for digit ”4”, where brighter colors indicate higher similarity values. These matrices show notably higher and more uniform similarity values in standardized view compared to both original and transformed views, as indicated by the consistently brighter colors.

These results validate that our Homography VAE successfully learns to generate consistent standardized view representations without explicit supervision of transformation parameters.

5 CONCLUSIONS

In this paper, we presented Homography VAE, a novel unsupervised framework for standardized view image reconstruction from multi-viewpoint input. Our main contributions include a novel architecture that incorporates Homography transformation into the VAE framework through coordinate transformation, enabling unsupervised learning of viewpoint transformations. We demonstrated that decomposing the latent space into feature and transformation compo-

(a) original image (b) transformed (c) standardized

Figure 3: Reconstruction results for MNIST digit "4". Given original input images with various viewpoint transformations (a), our model generates two types of reconstructions. (b) are transformed view reconstructions that preserve the original perspective of each input. (c) are standardized view reconstructions that align all outputs to a consistent frontal viewpoint. The results (c) demonstrate that our model successfully handles complex digit structures while maintaining consistent standardization of viewpoint.

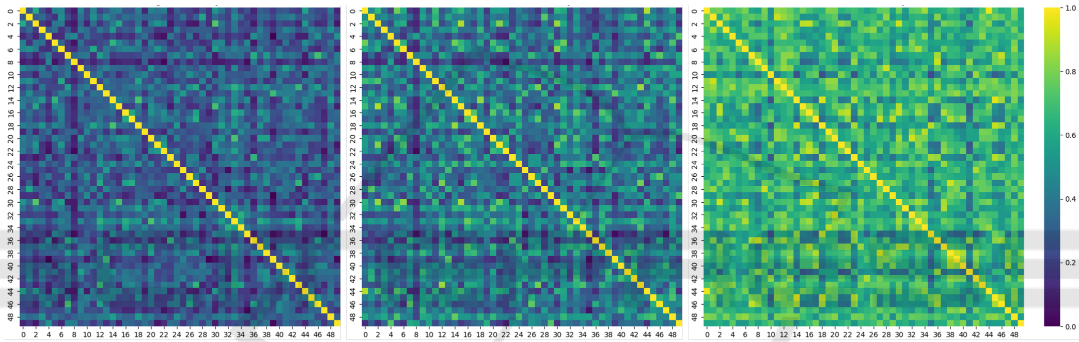

(a) original image (b) transformed (c) standardized

Figure 4: Visualization of pairwise cosine similarity matrices computed from 50 samples within the same class. Results shown are from MNIST digit "4". For each type of images ((a) original, (b) transformed reconstructions, and (c) standardized reconstructions), we compute the cosine similarity between all pairs of images. The color intensity represents the similarity value, where brighter colors indicate higher similarity. The more uniform and brighter patterns in (c) demonstrate that standardized reconstructions achieve consistently higher similarity across all pairs, validating the effectiveness of our approach in generating consistent representations.

nents allows for effective generation of both input and standardized view using a single framework. Furthermore, experimental results show that our method achieves significantly higher consistency in standardized view reconstruction compared to input and transformed views, without requiring ground truth Homography matrices.

For future work, extending our method to handle real-world scenes with multiple objects, varying lighting conditions, and higher resolution images would enhance its practical applications. Additionally, investigating more complex geometric transformations beyond Homography would further expand the capability of our framework.

REFERENCES

Bidart, R. and Wong, A. (2019). Affine variational autoencoders. In *Image Analysis and Recognition: 16th International Conference, ICIAR 2019, Waterloo, ON, Canada, August 27–29, 2019, Proceedings, Part I 16*, pages 461–472. Springer.

DeTone, D., Malisiewicz, T., and Rabinovich, A. (2016). Deep image homography estimation. *ArXiv*, abs/1606.03798.

Fu, H., Li, C., Liu, X., Gao, J., Celikyilmaz, A., and Carin, L. (2019). Cyclical annealing schedule: A simple approach to mitigating KL vanishing. In Burstein, J., Doran, C., and Solorio, T., editors, *Proceedings of the 2019 Conference of the North American Chapter of the Association for Computational Linguistics: Human Language Technologies, Volume 1 (Long and*

Short Papers), pages 240–250, Minneapolis, Minnesota. Association for Computational Linguistics.

Higgins, I., Matthey, L., Pal, A., Burgess, C. P., Glorot, X., Botvinick, M. M., Mohamed, S., and Lerchner, A. (2017). beta-vae: Learning basic visual concepts with a constrained variational framework. *ICLR (Poster)*, 3.

Jaderberg, M., Simonyan, K., Zisserman, A., et al. (2015). Spatial transformer networks. *Advances in neural information processing systems*, 28.

Kingma, D. P. and Welling, M. (2014). Auto-Encoding Variational Bayes. In *2nd International Conference on Learning Representations, ICLR 2014, Banff, AB, Canada, April 14-16, 2014, Conference Track Proceedings*.

Le, H., Liu, F., Zhang, S., and Agarwala, A. (2020). Deep homography estimation for dynamic scenes. In *Proceedings of the IEEE/CVF conference on computer vision and pattern recognition*, pages 7652–7661.

Pascanu, R., Mikolov, T., and Bengio, Y. (2013). On the difficulty of training recurrent neural networks. In Dasgupta, S. and McAllester, D., editors, *Proceedings of the 30th International Conference on Machine Learning*, volume 28 of *Proceedings of Machine Learning Research*, pages 1310–1318, Atlanta, Georgia, USA. PMLR.

Wang, C., Wang, X., Bai, X., Liu, Y., and Zhou, J. (2019). Self-supervised deep homography estimation with invertibility constraints. *Pattern Recognition Letters*, 128:355–360.